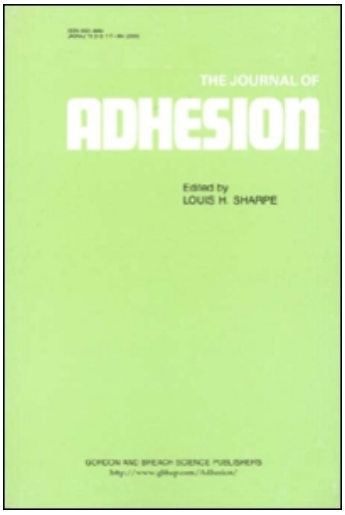

The Journal of Adhesion
Publication details, including instructions for authors and subscription information:
http://www.informaworld.com/smpp/title~content=t713453635

Evolution of Rim Instabilities in the Dewetting of Slipping Thin Polymer Films

Günter Reiter[a]
[a] Institut de Chimie des Surfaces et Interfaces, CNRS-UHA, Mulhouse Cedex, France

To cite this Article Reiter, Günter(2005) 'Evolution of Rim Instabilities in the Dewetting of Slipping Thin Polymer Films', The Journal of Adhesion, 81: 3, 381 — 395
To link to this Article: DOI: 10.1080/00218460590944747
URL: http://dx.doi.org/10.1080/00218460590944747

The Journal of Adhesion, 81:381–395, 2005

ISSN: 0021-8464 print/1545-5823 online
DOI: 10.1080/00218460590944747

Taylor & Francis
Taylor & Francis Group

Evolution of Rim Instabilities in the Dewetting of Slipping Thin Polymer Films

Günter Reiter
Institut de Chimie des Surfaces et Interfaces, CNRS-UHA, Mulhouse Cedex, France

Using optical microscopy, we investigated the amplification of instabilities of the moving rim which formed during dewetting of slipping polymer films. At the onset, the wavelength of the rim instability grew in time and proportional to the width of the rim. At later stages, these instabilities led to finger and subsequent droplet formation. Droplet size was found to be proportional to the width of the rim at break-off of droplets, which, in turn, was proportional to the initial film thickness. Our experiments suggest that the decrease of the dewetting velocity with increasing width of the rim is the key mechanism responsible for this instability. Droplet formation provided a possibility for self adjustment of the dewetting front resulting in a constant mean self-regulated dewetting velocity. This mean velocity was significantly higher than the velocity for the corresponding stable rim.

Keywords: Dewetting; Instabilities; Thin polymer films; Slippage; Fingering; Droplet formation

INTRODUCTION

Dewetting—the drying of a substrate covered with a liquid film—is a phenomenon found frequently in everyday life. Recently, it has attracted much scientific interest and a multitude of fundamental studies has

Received 5 October 2004; in final form 25 January 2005.

This paper is one of a collection of articles honoring Manoj Chaudhury, the recipient in February 2005 of *The Adhesion Society Award for Excellence in Adhesion Science, Sponsored by 3M*.

PACS numbers: 61.41.+e, 68.15.+e, 68.08.Bc, 68.03.Cd.

I am indebted to Philippe Auroy for providing me with the endfunctionalized PDMS-molecules. The help of Rajesh Khanna with experiments is highly appreciated. Fruitful discussions with Françoise Brochard, Jean-François Joanny, and Ashutosh Sharma are gratefully acknowledged.

Address correspondence to Günter Reiter, Institut de Chimie des Surfaces et Interfaces, CNRS-UHA, 15 Rue Jean Starcky, B.P. 2488, 68057 Mulhouse, Cedex, France. E-mail: g.reiter@uha.fr

been performed [1–7, 10–12]. Consequently, our understanding of the processes involved in this phenomenon is already well advanced. Nonetheless, there exist still several observations which are not yet fully explained. One such aspect concerns the instabilities of the retracting rim collecting the liquid from the already dewetted area. These instabilities lead to the formation of fingers and, eventually, of many small droplets.

When dewetting is initiated at a straight line, the resulting rim is a long but thin liquid ridge which has a form similar to a semi-cylinder. Based on analogies to the Rayleigh instability of an immobile liquid ridge, supported by experimentally observable undulations in height and width of the rim, theory [3, 13] expects that the rim formed in any dewetting experiment becomes unstable. However, in many, if not most, dewetting experiments using polymer films no such instabilities were observed [2, 4–6, 10–12]. Nonetheless, in a few of the early dewetting experiments [2, 3, 7–9], instabilities of the rim, similar to the formation of fingers, were found. We note that in contrast to the extensively studied fingering instabilities observed under the influence of centrifugal forces [14], thermal gradients [15–18], concentration gradients [19, 20], rim instablities in dewetting of highly volatile liquids [21] and fingering in elastic films [22, 23] no obvious gradients in acting forces or surface properties are involved in dewetting of polymers.

In a typical dewetting experiment of non-volatile liquids driven by capillary forces the velocity of the dewetting process results from balancing the driving forces by viscous forces with dissipation either concentrated in the wedge close to the contact line or proportional to the whole rim-substrate interface [1, 24, 25]. Capillary forces depend mostly on static properties and are typically time-independent. In contrast, dissipation may vary with time, e.g. if the frictional forces are proportional to the size of the moving liquid rim. Such is happening if the liquid "slips" on top of the substrate [24, 25] like in autophobic polymer dewetting, where a thin film of polymer melt dewets a densely end-grafted layer of identical polymers. This was shown in previous experiments [26]. There, the dewetting velocity decreased as the size of the rim increased.

In a previous short publication [27], it was demonstrated that the rim instability can be switched on and off by changing the film-substrate interfacial properties. The main conclusion of this study was that in the case of slippage the rim will become unstable and droplets will be formed. On the contrary, if there is no slippage, the rim will stay unbroken, possibly with some variation (sometimes even periodic) of its width and height along the contact line. In this study, the focus is on charcteristic features of the rim instabilities like the

thickness dependence of the characteristic wavelength. We give a detailed analysis of the local properties along the contact line like velocity or width of the rim. We also discuss the temporal evolution of the instability.

EXPERIMENTS

The present study is based on experiments using the previously well investigated poly-dimethylsiloxane (PDMS) system [26–30]. Thin films of long PDMS molecules (molecular weight $M_w = 308\,\mathrm{kg/mol}$, viscosity $\eta(25^\circ\mathrm{C}) = 1000\,\mathrm{Pa.s}$ or, alternatively, $M_w = 156\,\mathrm{kg/mol}$, $\eta(25^\circ\mathrm{C}) = 100\,\mathrm{Pa.s}$) of different thicknesses between 10 and 100 nm (as measured by ellipsometry) were spincoated on top of silicon substrates coated with densely grafted layers (polymer brushes) of short end-functionalized PDMS molecules.

Dense monomodal brushes were made from SiH monofunctionalized PDMS chains of uniform length (molecular weight $M_w = 8.8\,\mathrm{kg/mol}$, index of polydispersity $I_p = 1.07$). Prior to grafting, the silicon wafer (cleaned by UV ozone in a humid atmosphere) was treated with chlorodimethylvinylsilane to suppress adsorption of a PDMS and to functionalize the surface with vinyl groups. SiH-PDMS, diluted in heptane containing a platinum catalyst, was spin-coated onto the wafer. The resulting films were annealed at 120°C, allowing a chemical reaction (hydrosilation) between the SiH-end groups and the vinyl groups at the substrate. The samples were put into a bath of heptane to wash off all non grafted molecules. From the dry thickness (about $6.5 \pm 0.5\,\mathrm{nm}$), determined by ellipsometry, the grafting density of the brush chains ($0.44 \pm 0.04\,\mathrm{chains/nm^2}$) could be deduced.

PDMS films on such densely grafted brushes showed autophobic behavior [26, 28, 31]. All films were metastable and started to dewet at a straight three-phase contact line which was created by breaking the silicon substrate along a crystallographic axis in two parts [26]. In contrast to the opening of cylindrical holes like the ones investigated in [2], in the present case the length of the contact line was constant, at least on the average.

Dewetting was followed in real time by optical microscopy at 130°C. The samples were placed onto an enclosed hot stage (LINKAM THMS600), purged with nitrogen, under a Leitz-Metallux 3 optical microscope. No polarization or phase contrast was used. Contrast is due to the interference of the reflected white light at the substrate/film and film/air interface, resulting in well-defined interference colors which can be calibrated with a resolution of about 10 nm. We have followed the retraction of the three-phase contact line and the growth of

the rim in real time. Images were captured with a CCD camera. All data were stored with a VCR for later analysis. The thinnest films were also investigated at temperatures as low as room temperature to compensate for the increasing dewetting velocity with decreasing film thickness [26]. Taking into account the temperature dependence of the viscosity allowed to compare results from different temperatures in a quantitative way.

RESULTS AND DISCUSSION

In Figures 1 through 4 we present typical results of rim instabilities as a function of increasing film thickness. In addition, a comparison between Fig. 1 and Fig. 2 also shows that the viscosity (or molecular weight) of the dewetting polymer does not change the behavior qualitatively. As anticipated, the viscosity has a controlling influence (together with several other parameters [26]) on the velocity of the dewetting process but does not represent the cause for the instability of the rim. Several additional features have to be noted:

- Almost from the beginning of dewetting, the rim becomes wavy and shows rather periodic undulations in height and width.

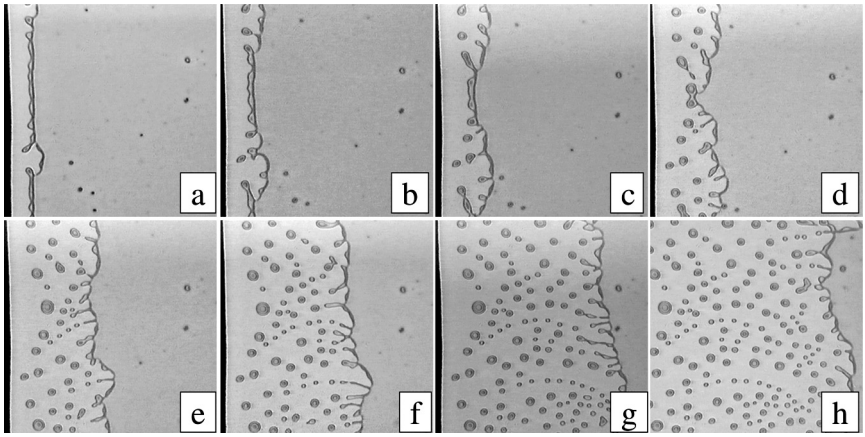

FIGURE 1 Optical micrographs for the retraction of a 22 nm thick PDMS (100 Pa.s) film at 130°C on a silicon wafer coated with a 6 nm grafted PDMS layer. Frames (a)–(h) were recorded after 24, 29, 34, 41, 53, 70, 86, and 107 sec, respectively. The dewetted area appears lighter than the film. Retraction started at the edge of the sample shown on the left side of the frames. The size of the images is $200 \times 200\,\mu m^2$. Frame (h) is shifted by 30 μm to the right with respect to the other frames.

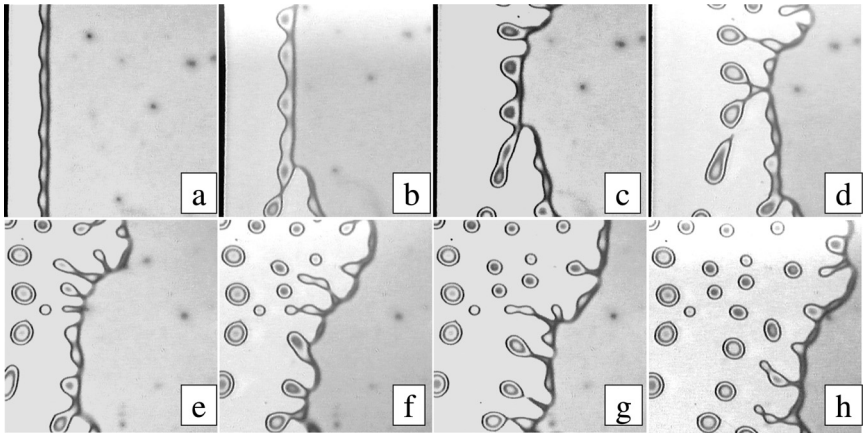

FIGURE 2 Optical micrographs for a 25 nm thick film and the same conditions as in Fig. 1. However, the polymer has a higher viscosity (1000 Pa.s) and the size of the images is now $80 \times 80\,\mu m^2$. Frames (a)–(h) were recorded after 45, 118, 165, 217, 249, 289, 375, and 502 sec, respectively. Frames (e)–(h) are shifted by 60 μm to the right with respect to frames (a)–(d).

- The undulations occurred at the front side of the rim, i.e. at the three phase contact line, while the rear side was still comparatively straight.

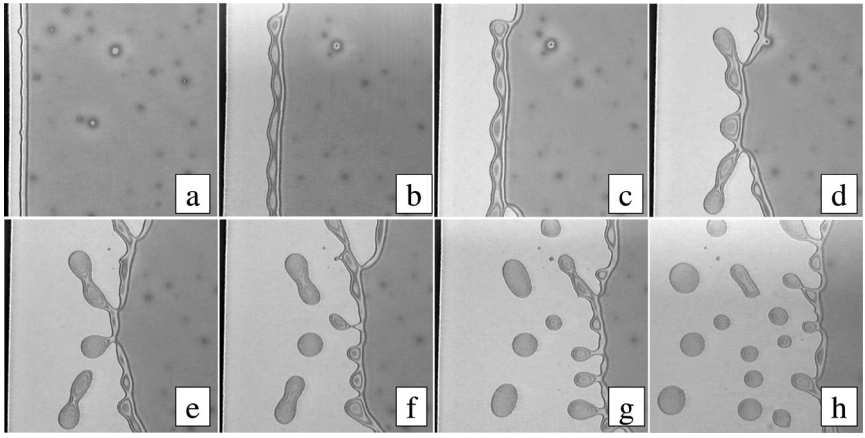

FIGURE 3 Optical micrographs for a 50 nm thick film and the same conditions as in Fig. 1. Frames (a)–(h) were recorded after 16, 94, 123, 181, 217, 258, 299, and 428 sec, respectively. The size of the images is $200 \times 200\,\mu m^2$. Frame (h) is shifted by 50 μm to the right with respect to the other frames.

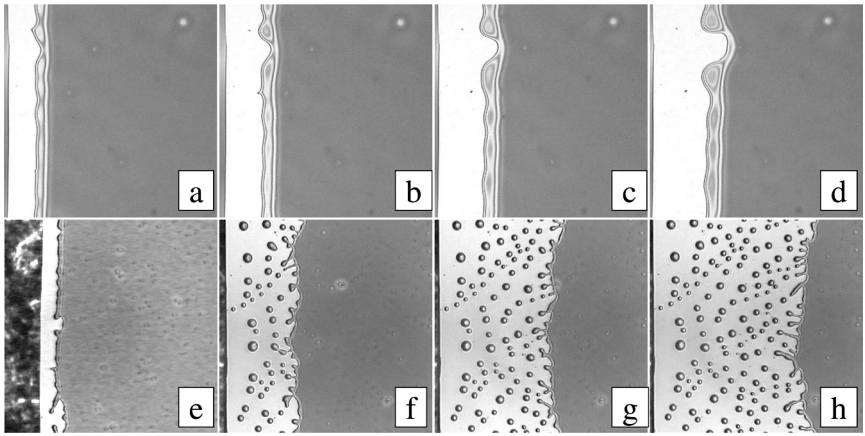

FIGURE 4 Optical micrographs for a 69 nm thick film and the same conditions as in Fig. 1. Frames (a)–(h) were recorded after 30, 50, 70, 90, 120, 480, 960, and 1200 sec, respectively. The size of the images is $200 \times 200\,\mu m^2$ for frames (a)–(d) and $800 \times 800\,\mu m^2$ for frames (e)–(h), respectively.

- Faster moving sections of the rim are always thinner than more slowly moving neighboring parts of the rim.
- The dewetted distance before the onset of droplet formation was larger for thicker films, i.e., the time for building up the first fingers increased with film thickness. Consequently, in experiments using much thicker films than investigated here no rim instabilities may be observed because the formation of fingers needs extremely long times.
- Dewetting could also proceed in the direction parallel to the rim, in particular at locations where the rim was rather thin. As a consequence, the periodicity of the initial undulations was destroyed. This caused also some polydispersity in the size of the final droplets.
- As dewetting proceeded, rim instabilities led to continuously repeated droplet formation, however in a somewhat irregular fashion.
- At late stages, a straight line, representing a mean dewetting front could easily be determined. Compared to the total dewetted distance, the local positions of the contact line fluctuated only by a rather small distance around this line. Thus, a mean dewetted distance, and accordingly a mean dewetting velocity, independent of the actual position along the contact line could be defined.
- Film thickness has a visible effect on the wavelength of the fingering instability and the size of the final droplets.

In Fig. 5 we give a typical example for the temporal evolution of the position d of the contact line. At the beginning the dewetted distance increased rather fast but its temporal increase slowed down as the width of the rim got larger. At later stages, when droplets were formed, we have determined the displacement of the mean position (d_{MEAN}) of the contact line. As can be clearly seen by comparison with the dotted lines representing the extrapolation of the initial behavior, droplet formation allowed to dewet larger distances (i.e., dewetting proceeded faster) as would have been possible without such an instability.

In Fig. 6, we show the velocity $V(t_i)$ of the dewetting process at time t_i, as determined by point-wise taking differences, $V(t_i) = (d(t_i) - d(t_{i-1}))/(t_i - t_{i-1})$, for three different samples. At times larger than about 200 sec we plotted V_{MEAN}, determined the same way by using d_{MEAN} instead of d. The large scatter of the data points arises mainly from the point-wise calculation of the velocities, amplifying the error

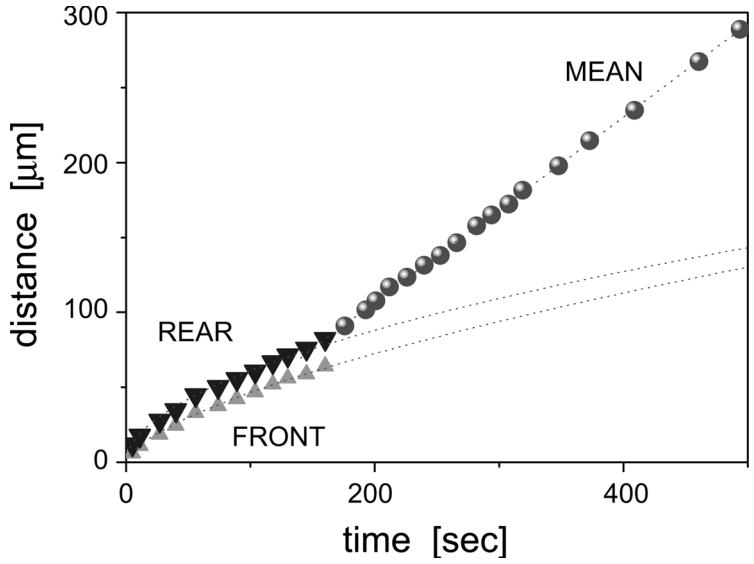

FIGURE 5 Time (t) dependence of the displacement of the rim for the sample shown in Fig. 3. At early times, the position of the front (F) and rear (R) side of the rim were recorded. At later times, the mean position of R-averaged over some 100 μm of length - was measured. It moved proportionally to $t^{1.08\pm0.05}$ (dotted line), i.e., at an almost constant velocity. In contrast, powerlaw fits to the measured data at early times, indicated by the dotted lines, yielded $F \sim t^{0.64\pm0.07}$ and $R \sim t^{0.58\pm0.06}$.

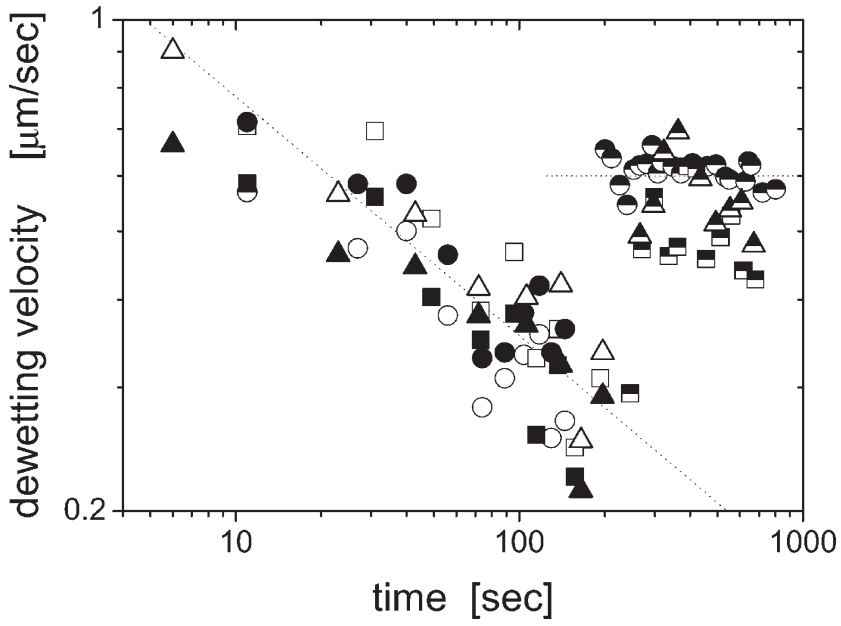

FIGURE 6 Double-logarithmic representation of the temporal (t) evolution of the dewetting velocity of the front (open symbols) and the rear (full symbols) side of the rim. The mean velocity at later times, averaged over a length of about 100 μm, is represented by the half-filled symbols. The thicknesses of the three samples are: 50 nm (circles), 69 nm (squares), and 71 nm (triangles). The dotted lines are guides to the eye and represent at early times a decreasing velocity v according to $v[\mu m\, s^{-1}] = 1.7[\mu m\, s^{-2/3}]t^{-1/3}$ and a constant velocity at later times $v = 0.6\mu m/s$.

bars of the individual measurements of $d(t_i)$. Initially the dewetting velocity was decreasing in time as expected for a system where the rim slips on the substrate [24]. Such a decay of V for slipping films has been investigated in detail in [26] for the system of the present study. Independent of film thickness, all three samples show qualitatively the same behavior. Quantitatively, however, the velocities are not the same for all samples. As studied in detail in [26], the prefactor contained in the relation describing the time-dependence of the dewetting velocity for an unperturbed rim is controlled by several parameters. Besides contact angle and viscosity these parameters are mainly film thickness and slippage length. In the here presented experiments, the slippage length was of the order of 10 μm. Thus, one may obtain the same dewetting velocity for samples of different thickness if the slippage length or the contact angle vary accordingly.

For the samples shown in Fig. 6 the viscosity and the contact angle ($7 \pm 1^\circ$) were the same but the slippage length differed slightly. Thus, the thickness dependence of the dewetting velocity is not clearly visible. A detailed study of the dependence of dewetting velocity on slippage length can be found in [26].

In contrast to the initially decreasing velocity, V_{MEAN} of the mean front at later stages is *constant*. Initially faster moving sections of the rim slowed down due to an increase of the width of the rim and initially slow parts accelerated by detaching droplets. As a consequence, the mean dewetting velocity, averaged over the time elapsing between the formation of successive droplets, is the same everywhere along the contact line. We note further that this constant velocity at late stages was back at the high value of the early stages when the rim was first built up.

In contrast to the *mean* velocity, we demonstrate in Fig. 7 that locally V was by no means constant. As the rim became wider, and eventually a droplet was formed, the velocity of this spot approached zero. As soon as a droplet got detached, this spot catched up with the rest of the contact line and the velocity jumped back to a high value. The displacement of the rim for the four adjacent spots shown in Fig. 7 clearly shows that their positions fluctuated around a linearly increasing value (corresponding to a constant velocity), indicated by the dotted line.

From our experiments, we may conclude that the initial small amplitude characteristic wavelength λ of the instability is likely set by the Rayleigh-mechanism (minimmisation of the surface energy). Such a mechanism predicts that λ is proportional to the width of the rim [3]. Our experiments showed that the wavelength of the undulation pattern of the rim, well *before* droplet formation, increased in time as the width of the rim grew. We give a characteristic example in Fig. 8. In an indirect way, λ also depended on film thickness. Thicker films have thicker rims right from the beginning. However, in contrast to thinner films the amplification of undulations in thicker films needed more time. Consequently, the dewetted distance was larger before the first droplets were detached. As shown in Fig. 9, a linear relation between λ and the width of the rim can be drawn at any time of the early stages of dewetting. It is even possible to superpose results from various film thicknesses. This is consistent with theortical expectations [3] based on analogies to the Rayleigh instability.

Finally, in Fig. 10 we show the influence of film thickness (h) on the *average* number (N) per $10^4\,\mu m^2$, and the related *average* distance between final droplets ($D[in\,\mu m] = 1/\sqrt{(N/10^4\,\mu m^2)}$), and the "average" width of the rim at the onset of break-off of droplets ($w_{break\text{-}off}$). Using mass conservation by comparing the volume of the dewetted

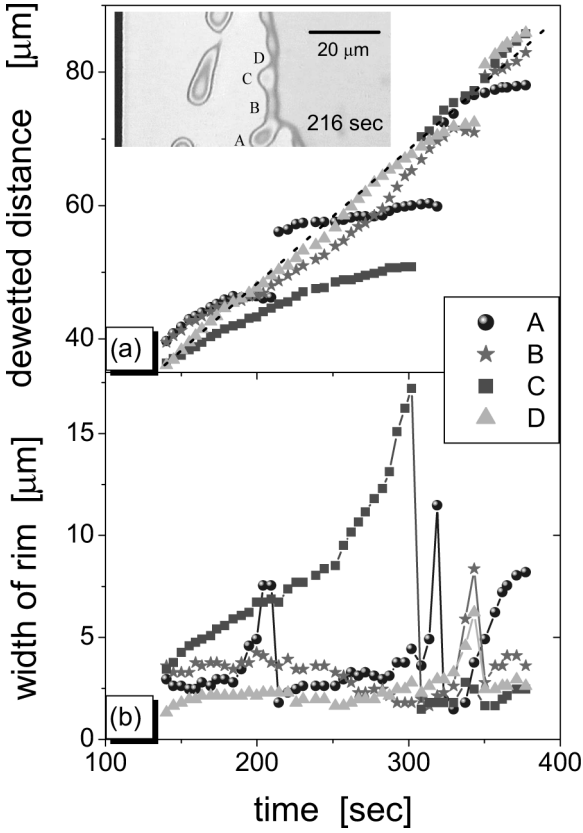

FIGURE 7 Spatial dependence of the temporal evolution of (a) the position of the three-phase contact line (=dewetted distance) and (b) the width of the rim for 4 locations (A–D, as indicated on the optical micropgraph in the inset of (a) for the sample shown in Fig. 2. Note that during the formation of the droplet at location C the width of the rim increases greatly while the contact line almost comes to a standstill until at around 300 sec the droplet detaches and the contact line catches up with the other locations. Note also the almost periodic detachment of droplets on location A. On the average, all locations move with a constant velocity as can be deduced from the approximately linear increase of the dewetted distance as seen in (a), indicated by the dotted line.

region with the volume of the resulting rim [24, 26], we can determine $w_{break\text{-}off}$:

$$w_{break\text{-}off}^2 = \frac{D \cdot h}{C \cdot \theta} \tag{1}$$

Here, the constant $C = 0.1$ accounts for the asymmetric shape of the rim [24].

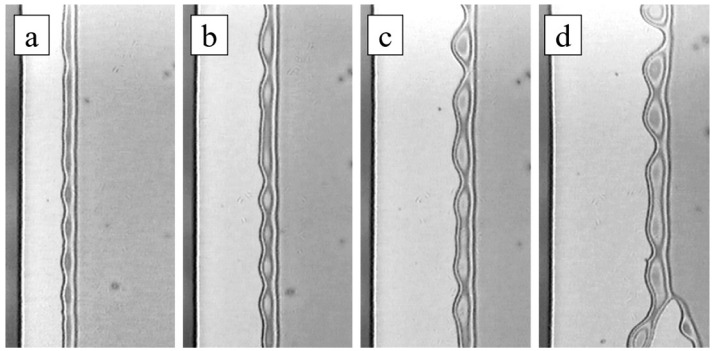

FIGURE 8 Representative optical micropgraphs (size: $100 \times 200\,\mu m^2$) showing the increase of the wavelength of the instability with time. The PDMS film (1000 Pa.s) is 49 nm thick and is dewetting on a 6 nm thick layer of endgrafted PDMS at 130°C. The times are 200, 506, 960, and 1170 sec for frames (a)–(d), respectively.

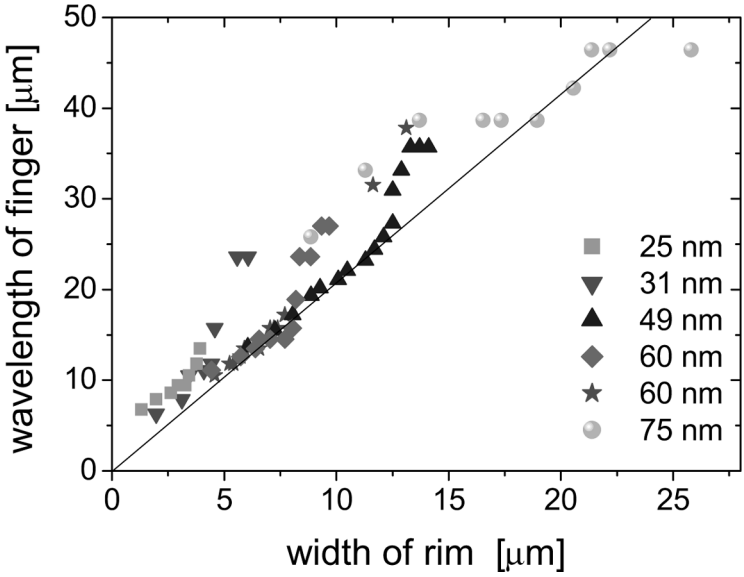

FIGURE 9 Average wavelength (λ) of the fingering instability as a function of the width (w) of the rim (which increased as dewetting progressed) for PDMS films of different thicknesses as indicated in the figure. The viscosity was 1000 Pa.s and the experiments were performed at 130°C. The full line acts as a guide to the eye indicating $\lambda = 2.1\,w$.

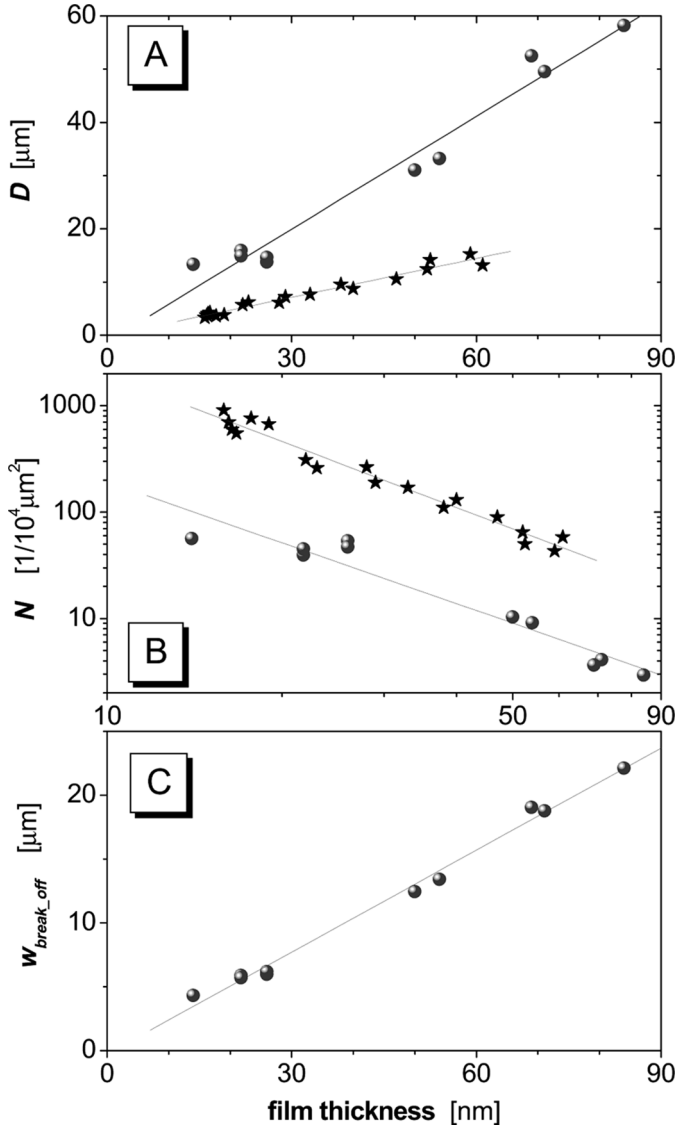

FIGURE 10 Dependence of (a) the mean distance (D) between final droplets, (b) the average number (N) of droplets per $10^4\,\mu m^2$, and (c) the mean width of the rim at break-off of droplets ($w_{break\text{-}off}$) as a function of film thickness (h). The results for the present PDMS system (circles) are compared with previously obtained results on polystyrene (PS) films (stars) [2]. The full lines represent best fits with the data and yield (all lengths are in μm) $D = -1.2 + 710 \pm 50\,h$, $N \sim h^{-1.90\pm0.19}$, $w_{break\text{-}off} = 0.27 + 270 \pm 10\,h$ and $D = -0.2 + 240 \pm 10\,h$, $N \sim h^{-2.06\pm0.09}$ for the PDMS and the PS system, respectively.

D increased about linearly with h and is also proportional to λ at break-off, once again indicating the analogy to the Rayleigh instability [3]. Accordingly, N was proportional to the inverse square of h. Most interestingly, $w_{break\text{-}off}$ was found to depend also linearly on h.

As indicated by the stars in Fig. 10, our observations are in accordance with earlier results on polystyrene (PS) films [2]. However, for PS D was increasing more slowly with h and accordingly, there were also more droplets per unit area. We attribute this difference to the significantly larger contact angle of about 40° for the PS system compared to about 10° for the PDMS system [26].

It can be seen that $D = 2.6 \pm 0.3 w_{break\text{-}off}$. This is roughly consistent with $D \approx \lambda$ at break-off (see Fig. 9: $\lambda = 2.1\,w$). Thus, the size of the final droplets is determined by the period of the undulations at break-off, which, in turn, is governed by the film thickness. Moreover, V_{MEAN} is controlled by $w_{break\text{-}off}$ and is a decreasing function of h (to be published).

We want to emphasize that it cannot be expected that the process of droplet formation results in a constant dewetting velocity. Alternatively, one could imagine that the dewetting front becomes very uneven, maybe even fractal-like and ramified. Such a diffuse front would not allow to define a mean velocity as no clear mean position of the front could be identified. However, the system chose to avoid uneven fronts with highly diverging velocities by detaching the most slowly moving parts of the rim in the form of droplets. Consequently, in the context of rim instabilities, the detachement of droplets represents a key process. It allows that wide and thus slowly moving sections of the rim to become thin enough to be able to catch up with the rest of the contact line.

This droplet detachment process has some reminiscence of avalanches sliding down a pile of sand (see e.g., [32]). V_{MEAN} would correspond to the angle of repose (θ) in the case of the sand pile. Both phenomena show signs of self adjustment of a certain parameter, either static (θ) or dynamic (V_{MEAN}), which optimizes the system. In our case, the system avoids slowing down of dewetting by making the rim unstable. In a first step the velocity becomes modulated corresponding to the thickness modulations of the rim. Thinner sections of the rim can move faster than the thicker parts, which evenyually will become fingers. Breaking-off droplets from fingers represents the second step in optimizing the dewetting velocity.

While the onset of the instability is most likely related to the Rayleigh instability (see Fig. 9, $\lambda = 2.1\,w$) this process alone cannot explain the observed behavior of a constant V_{MEAN}. Otherwise we would have to expect that in any dewetting experiment one would

observe finger formation at the rim. This is obviously not the case. The Rayleigh process alone is too slow to lead to fragmentation of the rim during its build up [33]. Thus, an additional mechanism is needed for a rapid amplification of the instability leading to a visible, continuous formation and subsequent fragmentation of fingers. We emphasize that we do not have a Marongoni type behavior as all interfacial tensions are constant. Most probably the amplifying mechanism is provided by the dependence of the dissipative term on the width of the rim, i.e., by a local increase (decrease) of the dewetting velocity with a local decrease (increase) in rim-width.

CONCLUSIONS

Our experiments clearly suggest that the dependence of the dewetting velocity on the width of the rim in the case of interfacial slippage is the basic underlying mechanism responsible for the spontaneous amplification of small fluctuations in the width of the rim which eventually lead to finger and subsequent droplet formation. The characteristic wavelength (λ) of the instability seems to be set by a Rayleigh-type mechanism implying that λ is proportional to the width (w) of the rim. Consequently, λ increased in the course of dewetting as the rim became larger. This amplification process for λ was stopped by the detachement of droplets when the rim reached $w_{break\text{-}off}$. Interestingly, $w_{break\text{-}off}$ was found to be proportional to the initial film thickness. Consequently, the time for droplet formation increased significantly with film thickness.

At present, it is not yet completely clear why this droplet formation process resulted in a *constant* average dewetting velocity although locally the dewetting velocity was by no means constant. It is, however, obvious that droplet formation provides a possibility for self adjustment of the the dewetting front, assuring a higher velocity than what one would have without such instability. One may call V_{MEAN} the self-regulated critical velocity of dewetting with slippage. Rim instabilities provide a mechanism for constant and, at the same time, much faster and thus highly effcient dewetting of the underlying substrate. As a general theme, in kinetic processes like the one here or in growth phenomena like diffusion limited aggregation [34], the velocity is optimized by an appropriate self-modulation of the resulting structure. It appears to be a general rule of Nature to choose the fastest and most efficient possibility at the expense of instabilities.

REFERENCES

[1] Redon, C., Brochard–Wyart, F., and Rondelez, F., *Phys. Rev. Lett.* **66**, 715–718 (1991).
[2] Reiter, G., *Phys. Rev. Lett.* **68**, 75–78 (1992); *Langmuir* **9**, 1344–1351 (1993).
[3] Brochard–Wyart, F. and Redon, C., *Langmuir* **8**, 2324 (1992).
[4] Shull, K. R. and Karis, T. E., *Langmuir* **10**, 334 (1994).
[5] Debrégeas, G., Martin, P., and Brochard-Wyart, F., *Phys. Rev. Lett.* **75**, 3886–3889 (1995).
[6] Lambooy, P., Phelan, K. C., Haugg, O., and Krausch, G., *Phys. Rev. Lett.* **76**, 1110–1113 (1996).
[7] Sharma, A. and Reiter, G., *J. Coll. Interf. Sci.* **178**, 383–399 (1996).
[8] Kim, H. I., Mate, C. M., Hannibal, K. A., and Perry, S. S., *Phys. Rev. Lett.* **82**, 3496–3499 (1999).
[9] van der Wielen, M. W. J., Baars, E. P. I., Giesbers, M., Cohen–Stuart, M. A., and Fleer, G. J., *Langmuir* **16**, 10137–10143 (2000).
[10] Pan, Q., Winey, K. I., Hu, H. H., and Composto, R. J., *Langmuir* **13**, 1758 (1997).
[11] Limary, R. and Green, P. F., *Langmuir* **15**, 5617 (1999).
[12] Yuan, C., Ouyang, M., and Koberstein, J. T., *Macromolecules* **32**, 2329 (1999).
[13] Leizerson, I., Lipson, S. G., and Lyushnin, A.V., *Langmuir* **20**, 291 (2004).
[14] Melo, F., Joanny, J. F., and Fauve, S., *Phys. Rev. Lett.* **63**, 1958–1961 (1989).
[15] Cazabat, A. M., Heslot, F., Troian, S. M., and Carles, P., *Nature* **346**, 824 (1990).
[16] Brzoska, J. B., Brochard-Wyart F., and Rondelez, F., *Europhys. Lett.* **19**, 97–102 (1992).
[17] Kataoka, D. E. and Troian, S. M., *J. Coll. Interf. Sci.* **192**, 350 (1997).
[18] Kataoka, D. E. and Troian, S. M., *Nature* **402**, 794 (1999).
[19] Troian, S. M., Herbolzheimer, E., and Safran, S. A., *Phys. Rev. Lett.* **65**, 333 (1990).
[20] Lee, S. H., Yoo, P. J., Kwon, S. J., and Lee, H. H., *J. Chem. Phys.* **121**, 4356–4351 (2004).
[21] Samid-Merzel, N., Lipson, S. G., and Tannhauser, D. S., *Phys. Rev.* **E 57**, 2906 (1998).
[22] Shull, K. R., Flanigan, C. M., and Crosby, A. J., *Phys. Rev. Lett.* **84**, 3057 (2000).
[23] Ghatak, A., Chaudhury, M. K., Shenoy, V., and Sharma, A., *Phys. Rev. Lett.* **85**, 4329 (2000).
[24] Brochard-Wyart, F., de Gennes, P. G., Hervert, H., and Redon, C., *Langmuir* **10**, 1566 (1994).
[25] Redon, C., Brzoska, J. B., and Brochard-Wyart, F., *Macromolecules* **27**, 468 (1994).
[26] Reiter, G. and Khanna, R., *Phys. Rev. Lett.* **85**, 2753–2756 (2000); *Langmuir* **16**, 6351 (2000).
[27] Reiter, G. and Sharma, A., *Phys. Rev. Lett.* **87**, 166103 (2001).
[28] Reiter, G. and Khanna, R., *Phys. Rev. Lett.* **85**, 5599 (2000).
[29] Reiter, G., Khanna, R., and Sharma, A., *Phys. Rev. Lett.* **85** 1432 (2000).
[30] Casoli, A., Brendlé, M., Schultz, J., Auroy, P., and Reiter, G., *Langmuir* **17**, 388 (2001).
[31] Leibler, L., Ajdari, A., Mourran, A., Coulon, G., and Chatenay, D., in *Ordering in Macromolecular Systems*, A. Teramoto, M. Kobayashi, and T. Norisuje (Eds.) (Springer-Verlag, Berlin, 1994), pp. 301–311.
[32] Turcotte, D. L., *Rep. Prog. Phys.* **62**, 1377 (1999).
[33] However, at the end of dewetting, after coalescence of holes, the resulting liquid threads always decompose into droplets according to the Rayleigh mechanism [2, 7].
[34] Brener, E., Müller-Krumbhaar, H., and Temkin, D., *Phys. Rev.* **E 54**, 2714 (1996).